



Provenance of the Late Permian Xuanwei Formation in the Upper Yangtze Block: Constraints from the Sedimentary Record and Tectonic Implications

ZHANG Yingli^{1,*}, JIA Xiaotong² and WANG Zongqi¹

¹ MNR Key Laboratory of Metallogeny and Mineral Assessment, Institute of Mineral Resources, Chinese Academy of Geological Sciences, Beijing 100037, China

² Engineering Seismology Institute of Zhejiang Province, Hangzhou 310013, China

Abstract: Xuanwei Formation is composed of mudstone, siltstone, and sandstone, with local conglomerate. However, its provenance and tectonic setting have been scarcely studied. In this paper, we use sedimentology, electron probe microanalysis (EPMA), and detrital zircon dating to investigate its source area and depositional tectonic setting. The facies assemblages indicate that it formed in alluvial fan and fluvial river sedimentary environments. The strata thicknesses and facies distribution indicate that the sediment supply was from the west. The results of EPMA show that chromian spinels within the sediments are characterized by high Cr[#] and varying Mg[#]. Discrimination plots suggest that these spinels were sourced from large igneous province (LIP) magmatic rocks. The laser ablation inductively coupled plasma mass spectrometry (LA-ICP-MS) U–Pb chronology of detrital zircons suggests that the sediments were derived from intermediate–acid igneous rocks dating back to 251–260 Ma. We could, therefore, conclude that the provenance of the Xuanwei Formation is from Emeishan basalt and synchronous felsic igneous rocks, which is consistent with the composition of the detrital framework. The detrital zircon dates also suggest that felsic magmatism occurred during the Late Permian, not after the eruption of the Emeishan basalt. Based on the sedimentary successions and provenance analysis, the tectonic setting for Xuanwei Formation deposition was a volcanic rifted margin.

Key words: Xuanwei Formation, provenance analysis, chromian spinel, detrital zircon geochronology, volcanic rifted margin

Citation: Zhang et al., 2019. Provenance of the Late Permian Xuanwei Formation in the Upper Yangtze Block: Constraints from the Sedimentary Record and Tectonic Implications. *Acta Geologica Sinica (English Edition)*, 93(6): 1673–1686. DOI: 10.1111/1755-6724.13866

1 Introduction

Large igneous provinces (LIPs) commonly include continental flood basalts (CFBs), oceanic plateaus, ocean basin flood basalts, and volcanic passive margins (Coffin and Eldholm, 1994). LIPs are characterized by the episodic emplacement of voluminous predominantly mafic rocks due to melting caused by hotspot activity (Ernst, 2014). Emeishan basalts are a prominent member of the world's LIPs, and considerable attention has therefore paid to their age (Fan et al., 2004; Zhong et al., 2007; Xu et al., 2008; Shellnutt et al., 2014), spatial distribution (He et al., 2007; Yang et al., 2015; Mabi et al., 2017), and associated dynamic mantle plume mechanism (Xu et al., 2001, 2008; He et al., 2006; Liu et al., 2009; Shellnutt et al., 2014, 2015).

Meanwhile, research on the Xuanwei Formation, which was deposited contemporaneously with the Emeishan basalts, has focused on the sedimentary environment, provenance analysis, and tectonic setting. Its sedimentary environments were divided into alluvial plain, lagoon, and tidal flat (Zheng et al., 2015) or alluvial plain, braided

river, delta, and tidal flat (Luo et al., 2008; Shao et al., 1994, 1998, 2013, 2016). The elemental composition of the Xuanwei Formation shale suggests that the sediments may have been derived from Emeishan basaltic rocks (Zhang et al., 2010). Felsic volcanic tuff interbedded with sandstones in the Xuanwei Formation has been attributed to alkaline felsic volcanism in the early Late Permian (He et al., 2007, 2010; Huang et al., 2016; Zhao et al., 2016). Detrital zircon LA-ICP-MS U–Pb dating of Xuanwei sandstone yielded ages ranging from 252 Ma to 2614 Ma, indicating a source in the Kangdian Oldland (He et al., 2017). However, only 41 spots have been dated, which is lower than the standard value (Andersen, 2002). Opinions regarding the Late Permian tectonic setting in the Upper Yangtze Block include a continental rift (Tan, 1987; Wang and Li, 1996; Wu, 1997; Ma et al., 2002; Song et al., 2004; Shellnutt and Zhou, 2008), a back-arc basin (Lepvrier et al., 2004; Jian et al., 2009), and a passive continental margin (Zhou and Liu, 1988; Xu et al., 1996; Yan and Wu, 1996) with a mantle plume (He et al., 2003).

Tectonic setting is the main factor controlling the sedimentary environment and provenance. Sedimentary successions and the distribution of sedimentary facies also

* Corresponding author. E-mail: yinglizh@126.com

reflect tectonic attributes. A heavy mineral composite may contribute data on provenance that is valuable for reconstructing the tectonic setting, as heavy minerals such as chromian spinels are more stable and less affected by transportation than other minerals (Cookenboo et al., 1997; Lee, 1999; Lenaz et al., 2009). Detrital zircon geochronology can constrain the formation age of parent rocks, and enable the correlation between tectonic units and reconstruction of the paleogeography (Du et al., 2017; Kang et al., 2018).

In this study, we investigate the sedimentology of the Xuanwei Formation of the Upper Yangtze to determine the sedimentary environment. We employ heavy mineral electron probe and U–Pb isotopic dating analyses to ascertain the provenance, source rocks, and tectonic setting of deposition. Our main objectives are to provide constraints on the source rock types and ages and their genetic relationship with Emeishan large igneous province (ELIP) rocks. We also discuss the tectonic setting of the Xuanwei Formation, including the influence of a mantle plume. The results of this study pave the way for further clarifying the tectonic evolution of the Yangtze Block, thus contributing to the understanding of the processes and geodynamic models responsible for the evolution of Kangdian Oldland.

2 Geological Background

The Upper Yangtze Block is separated from the Songpan-Ganzi Orogenic Belt and Simao Block by faults, such as the Longmenshan Fault and the Red River Fault (Fig. 1). The ELIP basalts (Fan et al., 2004; Zhong et al., 2007; Shellnutt et al., 2014; Xu et al., 2008) were emplaced in the Late Permian and are found in western Sichuan, northeastern Yunnan, and western Guizhou province (Fig. 1b). The thickness of Maokou Formation limestone erosion, seismic data, and crustal thickness have been used to divide the ELIP into three zones: an inner zone, an intermediate zone, and an outer zone (Chung et al., 1995; Xu et al., 2001, 2004, 2013; He et al., 2003) (Fig. 1b). The Xuanwei Formation disconformably underlies Emeishan basalts (Figs. 2a, 2b) and mainly consists of terrigenous clastic rocks, locally interlayered with tuff. The Xuanwei Formation is overlain by the Early Triassic Feixianguan Formation, which is mainly composed of coarse-grained sandstones intercalated with thin layers of mudstone.

3 Sedimentology

Five sections were examined in Xuanwei Formation outcrops. Section (a), (b), (c), and (d) are in the intermediate zone, whereas section (e) is in the outer zone (Fig. 1). All Xuanwei Formation successions were measured in the field at a centimeter-to-meter scale (Fig. 3). Field data were integrated with microfacies analysis and petrographic observations from 35 thin sections, resulting in the synthetic description of the identified facies is given in Table 1. The facies terms and codes refer to the scheme of Miall (1996). The grain size classification employs the Udden–Wentworth standard (Udden, 1914;

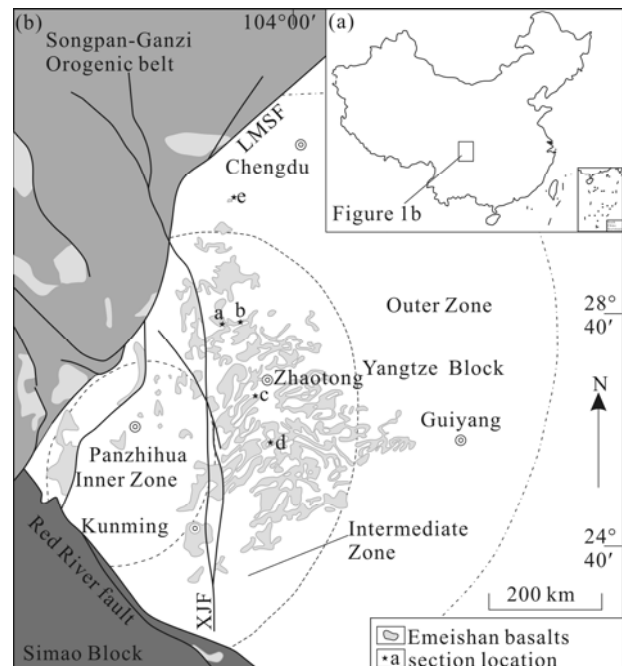


Fig. 1. Schematic geological map showing distribution of the Emeishan basalts, separation of inner, intermediate and the outer zone and section location of the Xuanwei Formation (after Xu et al., 2004; He et al., 2003)

LMSF-Longmenshan Fault, XJF-Xiaojiang Fault. China basemap after China National Bureau of Surveying and Mapping Geographical Information (a).

Wentworth, 1922).

3.1 Facies description and interpretation

Gmm. The facies is matrix-supported conglomerate (Fig. 2c). The matrix is reddish sandy siltstone and mudstone. Subangular breccias-with basalt and sandstone clasts are predominant. Poorly sorted units are 7.0–20.3 m thick (Fig. 3a), and do not show any grading. This facies is interpreted to have formed by redeposition of scoured floodplain sediment by turbulent hyperconcentrated flows (Shultz, 1984; Nemeč and Steel, 1984; Nemeč and Postama, 1993; Blair, 1999).

Gcm. This facies comprises clast-supported, structureless conglomerates. The conglomerates generally comprise subrounded to well-rounded clasts that range in size from granule to cobble. The gravels are mainly Emeishan basalt and fine-grained sandstone. The facies is commonly associated with siltstone and claystone. Its lower and upper boundaries are sharp to slightly scoured, and it displays lenticular geometries. The thickness of the conglomerate bodies reaches 6.2 m (Fig. 3c). The conglomerates are interpreted to have been formed by vertical accretion of lenticular bodies on longitudinal bars, probably in channels (Collinson, 1996; Miall, 1996).

Sh. This horizontally bedded medium-grained sandstone varies from 0.25 m to over 1 m in thickness. The sandstone is well sorted. Beds have sharp bases, and are commonly underlain by siltstone, claystone (Fm); and laminated sand, silt, and mud (Fl) (Fig. 2b). Current lineations occur in the bedding plane surface. This



Fig. 2. Typical field photographs of Xuanwei Formation in the Upper Yangtze Block (a) parallel unconformity between Emeishan basalts ($P_3\beta$) and Xuanwei Formation (P_3x); (b) parallel unconformity between the conglomerate of Xuanwei Formation (P_3x) and Emeishan basalts ($P_3\beta$). Arrows indicate unconformity; (c) massive matrix-supported conglomerate; (d) grey green horizontally fine-grained sandstone, underlying red mudstone; (e) grey green thinned-bedded siltstone and massive fine-grained sandstone; (f) grey red thinned-bedded siltstone and mudstone.

Table 1 Sedimentary facies of the Xuanwei Formation in the Upper Yangtze area

Facies code	General description	Sedimentary structures	Interpretation	References
Gcm	Clast-supported conglomerate, coarse-grained sandstone matrix. Basalt clasts are dominant, rare sandstone clasts are also present	Massive or crudely stratification	Vertical accretion under upper flow regime in aggrading channels	Rust, 1978
Gmm	Matrix-supported conglomerate, unsorted, well rounded, 2–8 cm sized clasts in siltstone to mudstone matrix. Units do not show any grading of clasts.	Massive bedding	Sediment gravity flow deposits emplaced mainly as debris flows	Nemec and Postma, 1993; Blair, 1999
Sh	Horizontally bedded sandstone	Fine-grained sandstones, moderately sorted, parallel bedding	Deposits originated via upper flow regime	Miall, 1996
Sm	Massive sandstone	Fine-grained sandstones	the result of deposition from a largely unconfined/hyperconcentrated flow during abrupt changes in flow speed	Martin and Turner, 1998; Flood, et al., 2014; Horn et al., 2018
Fm	Massive siltstone, claystone	Coal streak	Depositions from standing pools of water during low-stage channel abandonment	Miall, 1996
Fl	Laminated sand, silt and mud		Deposition from suspension and from weak traction current	Miall, 1996; Foix et al., 2013

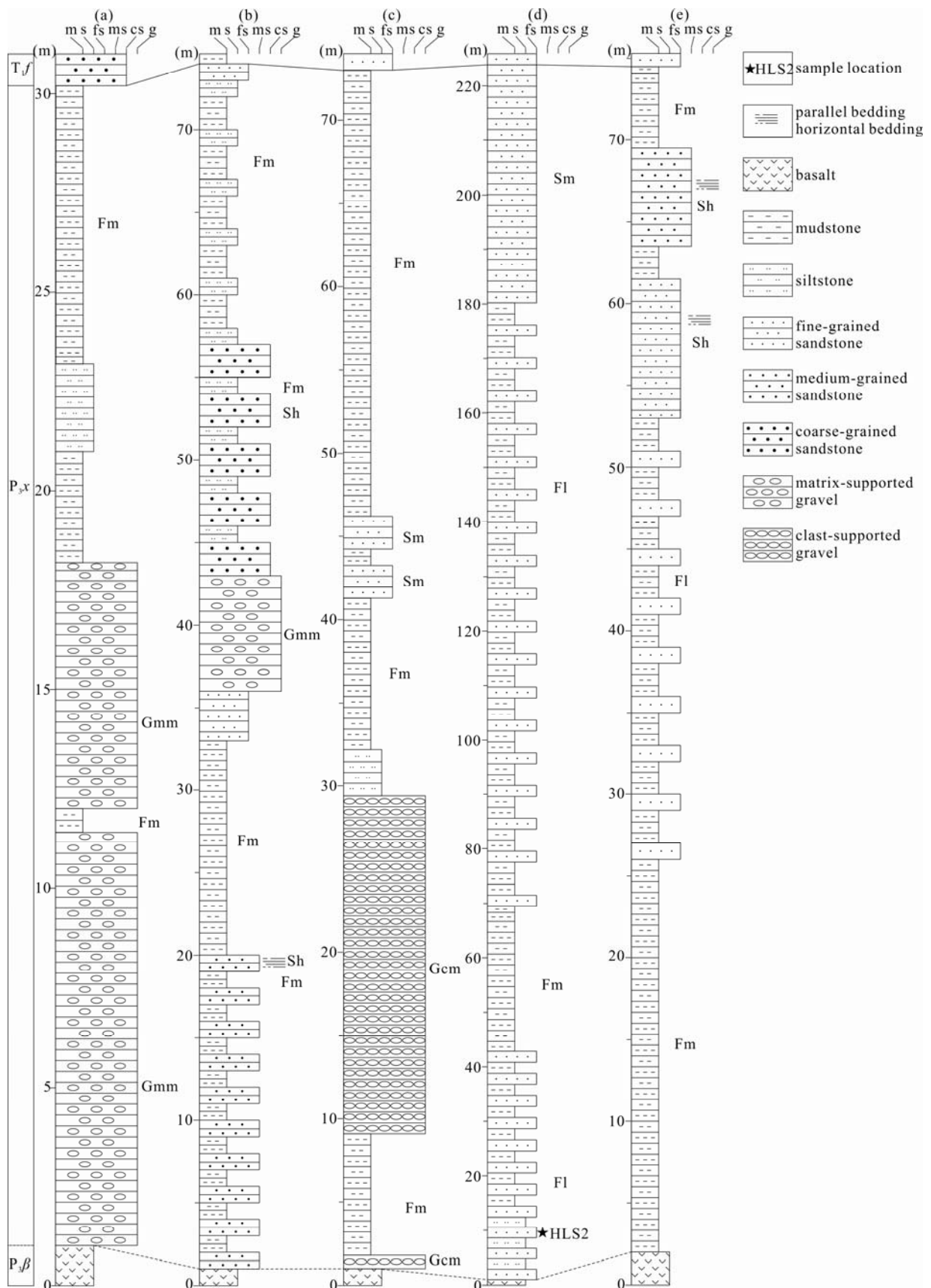


Fig. 3. Sedimentary successions of Xuanwei Formation in the Upper Yangtze area (section location in Fig. 1). Facies codes see text in detail.
 (a) Qingheng section; (b) Liuhong section; (c) Dalishu section; (d) Dajing section; (e) Yangziling section. See detail in Fig. 1.

sandstone is interpreted as upper flow plane-bed sands laid down as overbank sediments in stable sections of a river (Miall, 1996).

Fl. The facies is represented by fine-grained sandstone, siltstone, and claystone (Fig. 2e). The geometry of the beds is commonly sheet-like. Parallel laminations are the dominant physical sedimentary structures within sandstone and siltstone beds. Gray siltstoned and claystoned contain the remains of wood. The lower and upper boundaries are typically sharp. This facies is interpreted as low-energy deposits that accumulated in overbank areas during various flood stages. The dominant sedimentary process was suspension fallout accompanied by a periodic input of current-transported sands (Nadon, 1994).

Fm. The facies is represented by red and brown siltstone and mudstone (Fig. 2f). It is associated with the Sh and Fl facies but contains fewer preserved sedimentary structures than in the Sh and Fl facies. The vertical transition of the facies to Gcm, Gmm, Sl, and Sh indicates that this facies was deposited on an alluvial plain.

Sm. The facies is represented by massive, predominantly structureless sandstone. It displays erosive bounding surfaces where it is associated with facies Fsm or Fl. The facies is interpreted to be the result of deposition from a largely unconfined/hyperconcentrated flow during abrupt changes in flow speed (Martin and Turner, 1998; Flood and Hampson, 2014; Horn et al., 2018).

3.2 Section description and interpretation

(a) Qingheng section (28°04'57", 102°56'59")

The profile is mainly composed of purple–gray massive matrix-supported conglomerates (Gmm) and purple–red thinly bedded mudstone and siltstone (Fm). The gravels are mostly gray–green basalt clasts with 1–10 cm in diameter. Sorting is poor, and the clasts are well rounded to subrounded. The siltstone and mudstone have horizontal bedding and lenses of fine-grained sandstone. The section contains a combination of gravelly debris flow (Gmm) and deposition from suspensions (Fm). The depositional processes implied are typical of proximal alluvial fans dominated by mass movements alternating with flood-related plain (Nemec and Postma, 1993).

(b) Liuhong section (28°08'36", 103°10'40")

The lower part of the section is dominated by brown medium-bedded fine-grained sandstone (Sh) interbedded with mudstone (Fm). Sandstones show parallel bedding and commonly pass upward into red mudstone. The middle part of the section is represented by mudstone (Fm) and gray matrix-supported conglomerates (Gmm). The conglomerate beds are 60–80 cm thick and consist of matrix-supported pebbles. The conglomerate clasts are poorly sorted and well rounded. Medium-bedded coarse-grained sandstone (Sh) interbedded with mudstone (Fm) and siltstone and mudstone (Fm) occur in the upper part.

The lower and upper parts of the sequence are composed of horizontally stratified sandstone (Sh) and interbedded mudstone (Fm), characteristic of flash flood deposits. The Sh units would have been deposited when the hydrodynamic conditions of the flash flood were at the critical level (Miall, 1996), and the mudstone would have

been deposited when the flow weakened. Red mudstone and siltstone in the middle and upper sections are interpreted as the associated alluvial plain deposits. Matrix-supported conglomerates (Gmm) are interpreted as debris flows in an alluvial fan. This section records an alluvial system.

(c) Dalishu section (27°18'09", 103°24'14")

This section is mainly composed of siltstone and mudstone (Fm) interbedded with massive sandstone (Sm) and clast-supported conglomerates (Gcm). Red mudstone and siltstone are dominant in this section. The thickness of the conglomerates is 20.3 m. The conglomerates are clast-supported with a sandy matrix, are laterally discontinuous, and have a slightly scoured base. The upper and lower parts of the conglomerates contain fine-grained and coarse-grained sandstone lenses. Clasts are well rounded.

Thick red mudstone and siltstone, which are present in the lower and upper parts of the section, characterize an alluvial plain. The clast-supported conglomerates are interpreted as river deposits (Collinson, 1996; Miall, 1996).

(d) Dajing section (26°28'52", 103°47'33")

This section is principally characterized by laminated sandstone and mudstone (Fl) and mudstone (Fm). Massive sandstone (Sm) occurs at the top. Inferior coal is also seen at the bottom of the mudstone (Fl).

Except for the massive sandstone, the sediments are predominantly fine-grained. These siltstones and mudstones occur as thick, extensive beds containing the remains of freshwater plants and coal, indicating that they formed by suspension fallout in relatively large and long-lived standing bodies of freshwater. The massive sandstone is characteristic of a braided river (Martin and Turner, 1998). Therefore, this section records the following depositional processes: braided-stream flows (Sm) and suspension fallout in standing water (Fl, Fm).

(e) Yangziling section (29°49'36", 102°44'39")

This section is mainly composed of purple–red thinly bedded mudstone interlayered with fine-grained sandstone (Fm) and medium- to thickly bedded fine-grained sandstone and medium-grained sandstone (Sh). The fine-grained sandstone interlayered with mudstone exhibits a lenticular morphology. Sandstone (Sh) with parallel bedding contains a small amount of gravel at its bottom. The grain size of the sandstone fines upward. The superimposition relationship of the facies indicates that the sedimentary environment is a meandering river (Nemec and Steel, 1984). Facies Fsm and Fl were deposited on the floodplain, whereas the sandstones (Sh) were deposited in channels.

3.3 Sedimentary facies

Based on the field sections, the sediments were deposited in alluvial fan and river environments. The alluvial fan was in the middle zone of the ELIP, and the fluvial sediments were deposited in the middle–outer zone (Fig. 4), indicating that the sediment sources were from the west.

3.4 Petrology

The Xuanwei Formation sediments are mainly fine-

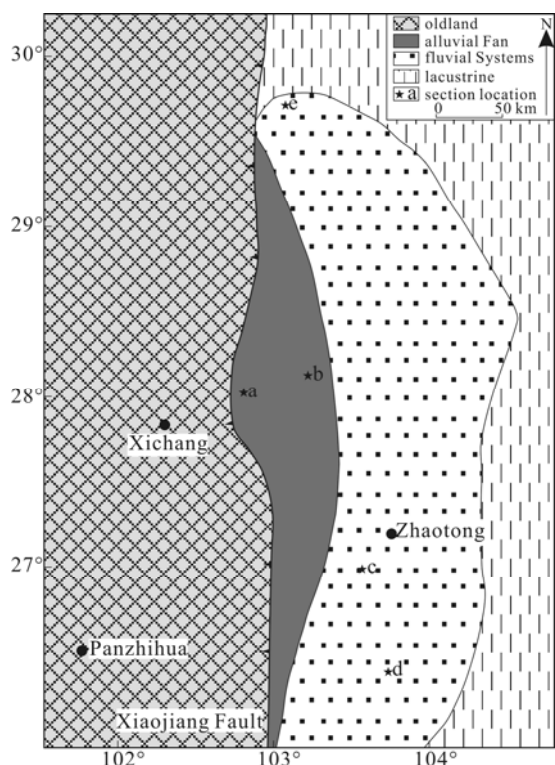


Fig. 4. Sedimentary facies distribution map of Xuanwei Formation in the Upper Yangtze block (modified from Shao et al., 2013; Ma et al., 2009).

grained. The conglomerates seen in the Qingheng and Liuhong sections consist mainly of Emeishan basalt and fine-grained sandstone.

Sandstone samples from the Xuanwei Formation are dominated by quartz grains and lithic fragments (Fig. 5). The quartz is dominantly monocrystalline. Feldspar is rare in the formation. The rock fragments are of volcanic rocks, both basic (Lvb) and felsic (Lva) (Fig. 5).

4 Sampling and Analytical Methods

4.1 Sampling

One sample of HLS2 from the Dajing section was examined under a microscope and then subjected to heavy mineral analysis (Fig. 2). The sample was crushed, screened, and separated at the Langfang Institute of Regional Geological and Mineral Survey, Hebei Province, China. The processed sample was divided into light minerals and heavy minerals (magnetic and nonmagnetic groups). Detrital heavy mineral grains (chromian spinels and zircon) were selected under the microscope for electron probe microanalysis (EPMA) and detrital zircon geochronology.

4.2 EPMA

The major element composition of detrital spinels was determined through wavelength-dispersive spectrometry using an EPMA-1600 electron probe microanalyzer at the University of China Geoscience (Beijing). The operating

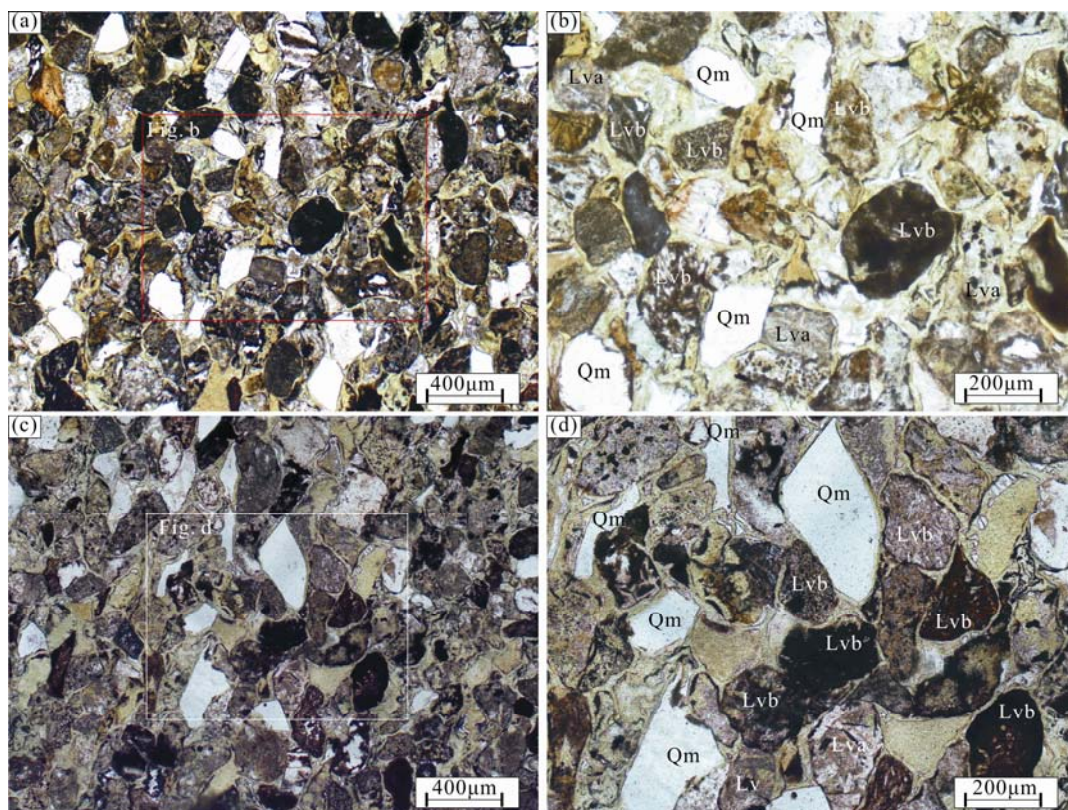


Fig. 5. Photomicroscopic image of Xuanwei Formation. (a) Quartz and basic magmatic rock fragments; (b) quartz with embayment and rock fragments image, showing that basic and acidic magmatic rocks. Q– monocrystalline quartz; Lvb– basic volcanic rock fragment; Lva–felsic volcanic rock fragment.

conditions were as follows: accelerating voltage=15 kV, beam current=10 nA, and beam diameter=1 μm . The following standards were employed: magnetite (Fe), albite (Si, Na, and Al), apatite (Ca, P), rutile (Ti), rhodonite (Mn), sanidine (K), olivine (Mg), fluorite (F), chromite (Cr), synthetic V_2O_3 , and pollucite (Rb, Cs). The EPMA results of the detrital spinels are presented in Table 2. The calculations were made using CALCMIN in Excel (Brandelik, 2009). The $\text{Mg}^\#$ and $\text{Cr}^\#$ parameters are defined as $\text{Mg}/(\text{Mg}+\text{Fe}^{2+})$ and $\text{Cr}/(\text{Cr}+\text{Al})$, respectively.

4.3 Detrital zircon U–Pb dating

The zircons were targeted by the Continental Dynamics Laboratory of the Institute of Geology, Chinese Academy of Geological Sciences. Zircon cathodoluminescence images were acquired using an S3000-N Hitachi scanning electron microscope equipped with a Chroma cathodoluminescence probe analysis instrument at Beijing Geoanalysis Co., Ltd. Detrital zircon LA-MC-ICP-MS U–Pb dating was carried out at the Laboratory of Geoanalysis and Geochronology, Tianjin Geological Survey Center, China. Please see the paper by Li et al. (2009) for details on the experimental testing processes. Data processing was conducted using ICPMSDataCal software (Liu et al., 2010), and the method of Anderson (2002) was adopted for common Pb correction.

Age interpretations are based on the $^{206}\text{Pb}/^{238}\text{U}$ age (Gehrels et al., 1999; Sircombe, 1999). The analytical data given in Table 3 are <20 % discordant on the basis of comparison of $^{206}\text{Pb}/^{238}\text{U}$ and $^{206}\text{Pb}/^{207}\text{Pb}$ ages (Gehrels et al., 1999; Nelson and Gehrels, 2007; Kalsbeek et al., 2008; Naipauer et al., 2010). The geochronological results were plotted on Concordia diagrams, histograms, and relative probability density plots using Isoplot 3.0 software (Ludwig, 2003).

5 Analytical Results

5.1 EPMA

Under the microscope, chromian spinels are dark, brown, and opaque and have an angular shape. Back-scattered images show no obvious nucleus–rim structure, which indicates that the spinels have been little affected by later metamorphism and alteration. The differences in the chemical compositions of chromian spinel particles are

mainly reflected in the parameters $\text{Mg}^\#$, $\text{Cr}^\#$, TiO_2 , and so on. The $\text{Mg}^\#$ values vary widely between 0.19 and 0.65. The $\text{Cr}^\#$ values are high, with a mean value of 0.75. The TiO_2 content is 1.23%–3.98 wt% (2.72 wt% on average). The probe results show that MnO and NiO have different correlations with $\text{Mg}^\#$. $\text{Mg}^\#$ and MnO are negatively correlated (correlation coefficient=–0.71), which suggests less alteration.

As the chromian spinels have >0.2 wt% TiO_2 and $\text{Fe}^{2+}/\text{Fe}^{3+}$ ratios of less than 4, they can be inferred to be mainly volcanic in origin (Lenaz et al., 2000) (Fig. 6a).

The TiO_2 and Al_2O_3 contents of most of the spinels plot with LIPs and in adjacent areas, with a few plotting with Ocean Island Basalt (Fig. 6b) (Kamenetsky et al., 2001). The TiO_2 content of spinels gradually increases in boninite, island arc basalt, intraplate basalt, ocean ridge basalt, and back-arc basin basalts, allowing magmatic affinity to be identified using Cr, Al, and Ti (Arai, 1992). In the TiO_2 and $\text{Cr}/(\text{Cr}+\text{Al})$ diagram (Fig. 6c), almost all of the spinels fall within the intraplate basalt field (oceanic hotspot basalts and flood basalts). In the Fe^{3+} –Cr–Al ternary diagram, all of the data fall in the CFB field (Fig. 6d).

Thus, the spinel analysis shows that the provenance of the Xuanwei Formation is mainly related to LIP/CFB volcanic rocks. The chromian spinels from the Xuanwei Formation studied here are closely consistent with spinels in the Emeishan basalt (Fig. 6). Therefore, Emeishan mafic suites, which were characterized as LIPs (Xu et al., 2001, 2007, 2008), may be the source area for sediments in the Upper Yangtze area.

5.2 Detrital zircon geochronology

The zircons analyzed are 150–300 μm in size and subangular in shape (Fig. 7). Their Th/U ratios range from 0.36 to 1.54. They display narrow and clear oscillatory zoning, indicating that the source rocks are felsic magmatic rocks (Rubatto and Gebauer, 2000; Corfu et al., 2003). Most of the CL images are dark (Fig. 7a), indicating high concentrations of U (Rubatto and Gebauer, 2000; Corfu et al., 2003).

We acquired 78 effective data points giving ages ranging from 253 ± 1 Ma to 260 ± 1 Ma. The 78 analyses form a tight cluster on the concordia diagram, yielding a weighted mean $^{206}\text{Pb}/^{238}\text{U}$ age of 256.7 ± 0.4 Ma (Fig. 8a).

Table 2 Chromian spinel electron probe data of Xuanwei sandstone HLS2 in the southwestern Upper Yangtze area (wt%)

Spot	SiO_2	TiO_2	Al_2O_3	Cr_2O_3	FeO	Fe_2O_3	MnO	MgO	NiO	Total	Si	Ti	Al	Cr	Fe^{3+}	Fe^{2+}	Mn	Mg	Ni	$\text{Mg}^\#$	$\text{Cr}^\#$
1	0.12	2.97	10.34	42.84	22.51	13.24	0.37	9.04	0.14	101.57	0.004	0.074	0.401	1.115	0.328	0.620	0.010	0.444	0.004	0.42	0.74
2	0.12	2.25	8.93	47.09	26.65	10.39	0.47	5.78	0.14	101.80	0.004	0.057	0.355	1.258	0.264	0.753	0.013	0.291	0.004	0.28	0.78
3	0.10	2.03	10.02	46.24	23.14	10.27	0.41	7.68	0.17	100.06	0.003	0.051	0.398	1.232	0.260	0.652	0.012	0.386	0.005	0.37	0.76
4	0.12	3.98	7.78	43.83	23.44	11.13	0.35	8.27	0.15	99.05	0.004	0.103	0.314	1.186	0.287	0.671	0.010	0.422	0.004	0.39	0.79
5	0.10	3.35	11.66	38.82	29.68	12.31	0.47	4.50	0.19	101.08	0.003	0.085	0.466	1.042	0.314	0.842	0.014	0.228	0.005	0.21	0.69
6	0.09	3.13	10.05	41.08	27.58	12.70	0.42	5.58	0.10	100.72	0.003	0.080	0.403	1.105	0.325	0.785	0.012	0.283	0.003	0.27	0.73
7	0.14	2.98	12.58	42.25	20.93	11.41	0.35	10.23	0.14	101.00	0.004	0.073	0.482	1.085	0.279	0.569	0.009	0.495	0.004	0.47	0.69
8	0.19	2.83	11.45	43.17	24.17	9.91	0.45	7.72	0.11	100.00	0.006	0.071	0.452	1.143	0.250	0.677	0.013	0.385	0.003	0.36	0.72
9	0.21	2.59	8.75	46.72	26.52	8.86	0.48	5.78	0.08	99.98	0.007	0.067	0.354	1.269	0.229	0.762	0.014	0.296	0.002	0.28	0.78
10	0.12	3.21	9.69	40.67	20.86	15.44	0.34	9.94	0.17	100.44	0.004	0.080	0.379	1.067	0.386	0.579	0.009	0.491	0.004	0.46	0.74
11	0.21	2.50	11.88	37.65	25.38	17.39	0.47	7.30	0.13	102.91	0.007	0.062	0.459	0.975	0.429	0.695	0.013	0.357	0.003	0.34	0.68
12	0.18	2.92	11.73	41.59	19.98	13.41	0.31	10.75	0.16	101.01	0.006	0.071	0.449	1.069	0.328	0.543	0.009	0.521	0.004	0.49	0.70
13	0.18	3.00	8.43	46.90	21.98	10.16	0.38	8.91	0.25	100.17	0.006	0.076	0.334	1.246	0.257	0.618	0.011	0.446	0.007	0.42	0.79
14	0.18	3.82	11.33	40.40	22.17	12.19	0.31	9.52	0.41	100.32	0.006	0.095	0.441	1.055	0.303	0.612	0.009	0.468	0.011	0.43	0.71
15	0.14	4.45	8.60	42.44	22.34	13.60	0.34	9.93	0.18	102.02	0.005	0.110	0.333	1.102	0.336	0.614	0.009	0.486	0.005	0.44	0.77

Note: Fe_2O_3 calculation based on the stoichiometric ratio of spinel.

Table 3 Detrital zircon U-Pb isotopic data from the Xuanwei Formation in the Upper Yangtze area

Spot	Element content (ppm)			Th/U ratio	Isotopic ratios						Age (Ma)				Conc. (%)		
	Pb	Th	U		$^{207}\text{Pb}/^{206}\text{Pb}$	1σ	$^{207}\text{Pb}/^{235}\text{U}$	1σ	$^{206}\text{Pb}/^{238}\text{U}$	1σ	$^{207}\text{Pb}/^{206}\text{Pb}$	1σ	$^{207}\text{Pb}/^{235}\text{U}$	1σ		$^{206}\text{Pb}/^{238}\text{U}$	1σ
1	13	282	305	0.93	0.0525	0.0007	0.2931	0.0047	0.0405	0.0002	307	28	261	4	256	1	102
2	18	226	446	0.51	0.0508	0.0004	0.2817	0.0033	0.0402	0.0002	231	18	252	3	254	1	99
3	19	233	458	0.51	0.0513	0.0005	0.2845	0.0035	0.0402	0.0002	255	19	254	3	254	1	100
4	18	238	446	0.53	0.0523	0.0004	0.2903	0.0034	0.0403	0.0002	297	18	259	3	254	1	102
5	15	202	360	0.56	0.0532	0.0005	0.2959	0.0041	0.0404	0.0002	336	21	263	3	255	1	103
6	18	205	418	0.49	0.0521	0.0005	0.2901	0.0037	0.0404	0.0002	290	21	259	3	255	1	102
7	19	210	447	0.47	0.0518	0.0004	0.2873	0.0034	0.0402	0.0002	278	17	256	3	254	1	101
8	21	250	499	0.50	0.0512	0.0004	0.2835	0.0032	0.0401	0.0002	251	18	253	3	254	1	100
9	19	193	463	0.42	0.0508	0.0004	0.2815	0.0032	0.0402	0.0002	230	17	252	3	254	1	99
10	21	259	506	0.51	0.0507	0.0004	0.2808	0.0031	0.0402	0.0002	228	17	251	2	254	1	99
11	6	115	145	0.79	0.0525	0.0018	0.2917	0.0113	0.0402	0.0002	306	76	260	9	254	1	102
12	15	162	372	0.43	0.0516	0.0007	0.2860	0.0051	0.0402	0.0002	267	30	255	4	254	1	100
13	20	247	498	0.50	0.0502	0.0007	0.2790	0.0051	0.0403	0.0002	202	31	250	4	255	1	98
15	11	107	284	0.38	0.0526	0.0010	0.2934	0.0070	0.0404	0.0002	313	42	261	6	255	1	102
16	19	226	463	0.49	0.0491	0.0010	0.2757	0.0069	0.0407	0.0002	152	45	247	5	257	1	96
17	18	214	442	0.49	0.0513	0.0010	0.2846	0.0069	0.0402	0.0002	255	41	254	5	254	2	100
18	17	187	413	0.45	0.0490	0.0009	0.2730	0.0061	0.0404	0.0002	147	40	245	5	255	1	96
19	15	272	345	0.79	0.0502	0.0008	0.2780	0.0061	0.0401	0.0002	202	37	249	5	254	1	98
20	19	294	460	0.64	0.0514	0.0007	0.2844	0.0049	0.0401	0.0002	258	28	254	4	254	1	100
22	56	715	1395	0.51	0.0521	0.0004	0.2890	0.0031	0.0402	0.0002	290	15	258	2	254	1	102
25	22	255	557	0.46	0.0536	0.0005	0.2966	0.0032	0.0401	0.0001	354	19	264	3	254	1	104
29	24	323	581	0.56	0.0509	0.0005	0.2816	0.0035	0.0401	0.0001	236	23	252	3	254	1	99
30	55	714	1391	0.51	0.0513	0.0002	0.2852	0.0014	0.0403	0.0001	255	6	255	1	255	1	100
31	58	685	1443	0.47	0.0510	0.0002	0.2834	0.0015	0.0403	0.0001	240	7	253	1	255	1	99
32	18	216	461	0.47	0.0542	0.0006	0.2993	0.0041	0.0400	0.0001	381	23	266	3	253	1	105
33	26	341	643	0.53	0.0505	0.0005	0.2788	0.0032	0.0401	0.0001	216	20	250	3	253	1	99
34	22	263	529	0.50	0.0531	0.0004	0.2952	0.0028	0.0404	0.0001	332	16	263	2	255	1	103
36	41	750	935	0.80	0.0508	0.0003	0.2833	0.0018	0.0404	0.0001	233	11	253	1	256	1	99
37	24	339	589	0.58	0.0516	0.0003	0.2880	0.0024	0.0405	0.0001	269	14	257	2	256	0	101
38	25	314	608	0.52	0.0513	0.0004	0.2860	0.0026	0.0404	0.0001	254	15	255	2	256	1	100
39	22	279	550	0.51	0.0515	0.0004	0.2858	0.0030	0.0403	0.0001	263	17	255	2	254	1	100
40	21	244	516	0.47	0.0519	0.0004	0.2901	0.0029	0.0406	0.0001	281	17	259	2	256	1	101
41	18	207	448	0.46	0.0499	0.0004	0.2794	0.0032	0.0406	0.0001	188	19	250	3	257	1	97
42	16	282	344	0.82	0.0523	0.0004	0.2943	0.0035	0.0408	0.0002	300	19	262	3	258	1	102
43	57	634	1434	0.44	0.0546	0.0002	0.3026	0.0018	0.0402	0.0001	395	7	268	1	254	1	106
44	18	220	452	0.49	0.0517	0.0007	0.2899	0.0045	0.0406	0.0001	274	30	259	4	257	1	101
45	70	877	1678	0.52	0.0513	0.0001	0.2876	0.0013	0.0407	0.0001	253	5	257	1	257	1	100
46	16	175	391	0.45	0.0506	0.0005	0.2849	0.0035	0.0409	0.0001	221	22	255	3	258	1	99
47	25	310	585	0.53	0.0509	0.0004	0.2859	0.0028	0.0407	0.0001	237	15	255	2	257	1	99
48	46	583	1116	0.52	0.0510	0.0002	0.2864	0.0018	0.0408	0.0001	240	10	256	1	258	1	99
49	14	183	337	0.54	0.0524	0.0006	0.2941	0.0038	0.0407	0.0001	302	24	262	3	257	1	102
50	32	573	742	0.77	0.0546	0.0004	0.3041	0.0027	0.0404	0.0001	396	15	270	2	255	1	106
51	12	164	300	0.55	0.0523	0.0006	0.2904	0.0040	0.0403	0.0001	298	24	259	3	255	1	102
52	18	221	430	0.51	0.0511	0.0005	0.2854	0.0036	0.0405	0.0001	246	23	255	3	256	1	100
53	9	195	186	1.05	0.0538	0.0019	0.3016	0.0119	0.0406	0.0002	364	80	268	9	256	1	105
54	18	232	448	0.52	0.0495	0.0005	0.2741	0.0033	0.0402	0.0001	170	23	246	3	254	1	97
55	18	211	433	0.49	0.0517	0.0005	0.2880	0.0032	0.0404	0.0001	273	20	257	3	255	1	101
56	20	275	477	0.58	0.0532	0.0005	0.2953	0.0035	0.0403	0.0001	335	21	263	3	255	1	103
57	15	185	383	0.48	0.0523	0.0007	0.2892	0.0043	0.0401	0.0001	299	28	258	3	253	1	102
58	14	161	355	0.45	0.0558	0.0005	0.3128	0.0037	0.0407	0.0001	444	20	276	3	257	1	107
59	15	172	374	0.46	0.0545	0.0004	0.3044	0.0033	0.0405	0.0001	390	18	270	3	256	1	105
60	18	216	435	0.50	0.0520	0.0004	0.2909	0.0032	0.0406	0.0001	287	19	259	3	256	1	101
61	16	188	401	0.47	0.0545	0.0006	0.3067	0.0041	0.0408	0.0001	390	24	272	3	258	1	105
62	16	199	379	0.52	0.0514	0.0006	0.2909	0.0042	0.0410	0.0001	259	26	259	3	259	1	100
63	14	177	358	0.49	0.0511	0.0008	0.2856	0.0052	0.0405	0.0001	247	36	255	4	256	1	100
64	10	168	260	0.64	0.0554	0.0009	0.3095	0.0061	0.0405	0.0001	430	37	274	5	256	1	107
65	15	163	371	0.44	0.0544	0.0005	0.3065	0.0036	0.0409	0.0001	387	21	271	3	258	1	105
67	3	62	61	1.01	0.0498	0.0036	0.2809	0.0220	0.0407	0.0003	185	160	251	17	257	2	98
68	19	242	469	0.52	0.0501	0.0003	0.2795	0.0027	0.0405	0.0002	197	15	250	2	256	1	98
69	16	189	401	0.47	0.0510	0.0004	0.2875	0.0034	0.0409	0.0002	239	20	257	3	259	1	99
70	25	327	623	0.52	0.0516	0.0002	0.2899	0.0024	0.0408	0.0002	267	10	258	2	258	1	100
71	20	314	483	0.65	0.0511	0.0005	0.2849	0.0036	0.0405	0.0001	243	23	255	3	256	1	100
72	18	294	426	0.69	0.0514	0.0004	0.2873	0.0033	0.0405	0.0002	260	17	256	3	256	1	100
73	3	43	79	0.55	0.0547	0.0024	0.3067	0.0149	0.0407	0.0002	399	98	272	12	257	1	106
74	20	240	499	0.48	0.0524	0.0003	0.2917	0.0030	0.0404	0.0002	303	14	260	2	255	1	102
75	16	476	310	1.54	0.0494	0.0005	0.2766	0.0043	0.0406	0.0003	166	23	248	3	257	2	96
76	54	682	1333	0.51	0.0513	0.0001	0.2906	0.0017	0.0411	0.0002	252	6	259	1	260	1	100
77	19	212	454	0.47	0.0517	0.0003	0.2884	0.0029	0.0405	0.0002	273	14	257	2	256	1	100
78	17	198	411	0.48	0.0530	0.0003	0.2970	0.0030	0.0407	0.0002	329	14	264	2	257	1	103
79	40	529	978	0.54	0.0510	0.0002	0.2870	0.0019	0.0408	0.0002	241	7	256	2	258	1	99
80	34	606	772	0.78	0.0518	0.0002	0.2924	0.0021	0.0410	0.0002	274	9	260	2	259	1	100
81	6	63	153	0.41	0.0542	0.0015	0.3071	0.0094	0.0411	0.0002	378	60	272	7	260	1	105
82	14	170	343	0.50	0.0512	0.0005	0.2896	0.0038	0.0410	0.0002	250	22	258	3	259	1	100
84	16	145	398	0.36	0.0513	0.0004	0.2871	0.0031	0.0406	0.0002	253	16</					

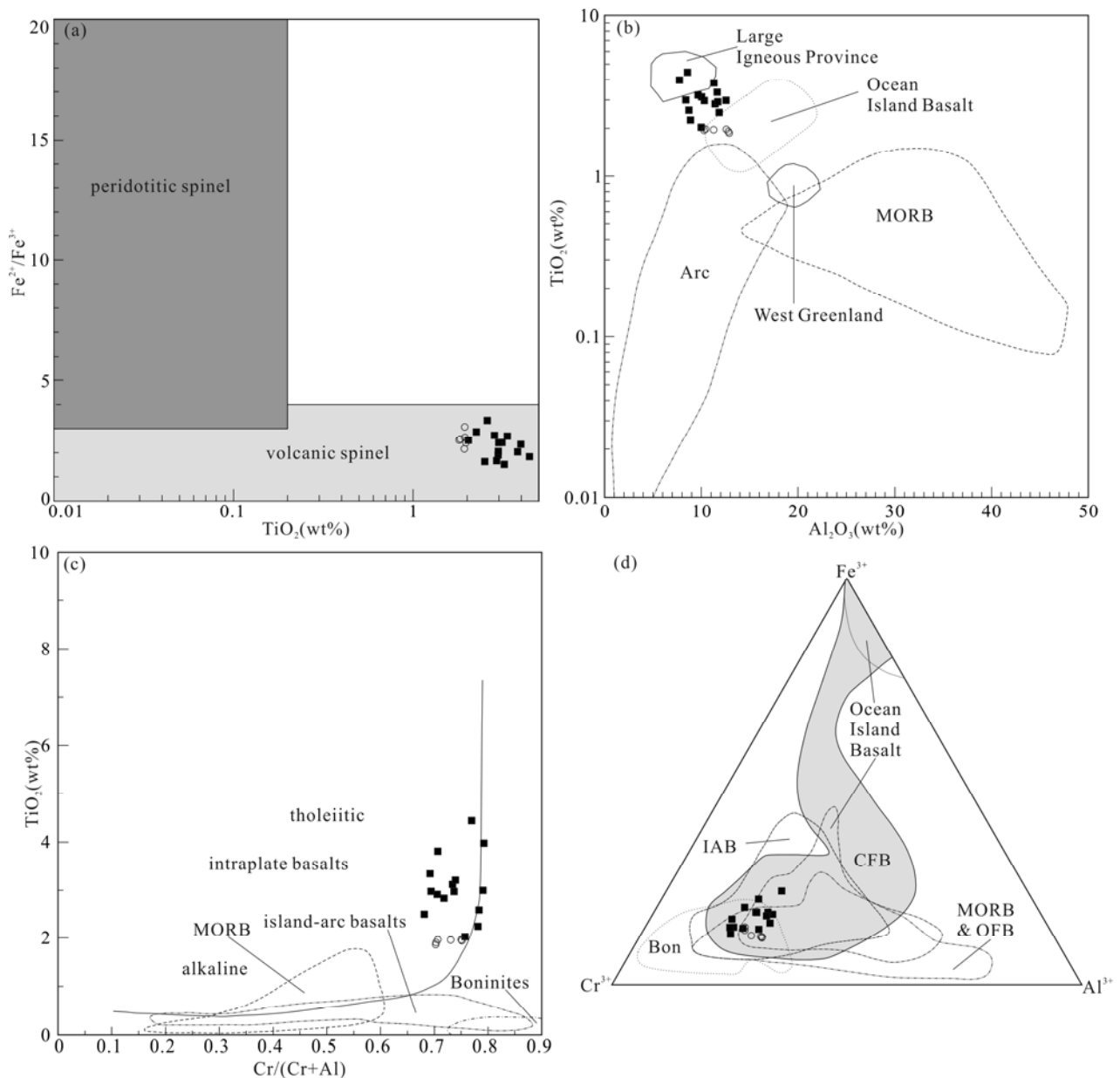


Fig. 6. Discrimination diagrams of detrital spinels composition from the Xuanwei Formation in the Upper Yangtze area (a) TiO_2 - $\text{Fe}^{2+}/\text{Fe}^{3+}$ diagram, compositional fields are after Lenaz et al. (2000); (b) Al_2O_3 - TiO_2 diagram, compositional fields are after Kamenetsky et al. (2001). (c) $\text{Cr}/(\text{Cr}+\text{Al})$ - TiO_2 diagram, compositional fields are after Arai (1992); (d) Fe^{3+} - Cr - Al diagram for discriminating different type volcanic spinels (Barnes and Roeder, 2001). Circle (○) data are adopted from Zhang and Wang (2004). MORB—Mid-ocean ridge basalt; IAB—Island arc basalt; Bon—Boninite; OFB—Ocean floor basalt; CFB—Continental flood basalt.

The histogram shows three peak values at 254 Ma, 256 Ma, and 258 Ma (Fig. 8b).

6 Discussions

6.1 Provenance

The Xuanwei Formation is mainly composed of gray-green mudstone and silty fine-grained sandstone (Figs. 2 and 3). Later tectonic movement has impeded the preservation of crossbedding from which to infer the paleocurrent direction. The thickness of the Xuanwei Formation gradually increases from the northwest [Sections (a), (b), and (e)] to the southeast [Sections (c)

and (d)], and basaltic breccia is present at the bottom in the western area [Section (a)], suggesting that the provenance of the sediments was from the northwest or the west. This is consistent with the provenance direction provided by the lithofacies and paleogeography (Fig. 4; Shao et al., 2013).

Quartz with a euhedral shape, embayments, unit extinction, and scarce inclusions (Fig. 5) is indicative of an extrusive igneous provenance. The rock fragments are basic and felsic igneous rocks (Fig. 5), suggesting that the source rocks are magmatic.

EPMA of chromian spinels also indicates that the source was mainly LIP rocks.

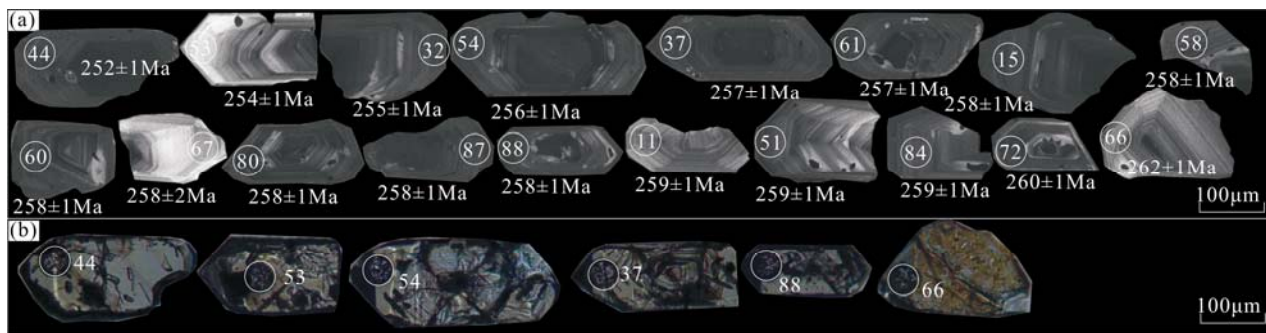


Fig. 7. LA-ICP-MS zircon U-Pb representative cathodoluminescence (CL) (a) and microscopic images (b) from the sample (HLS2).

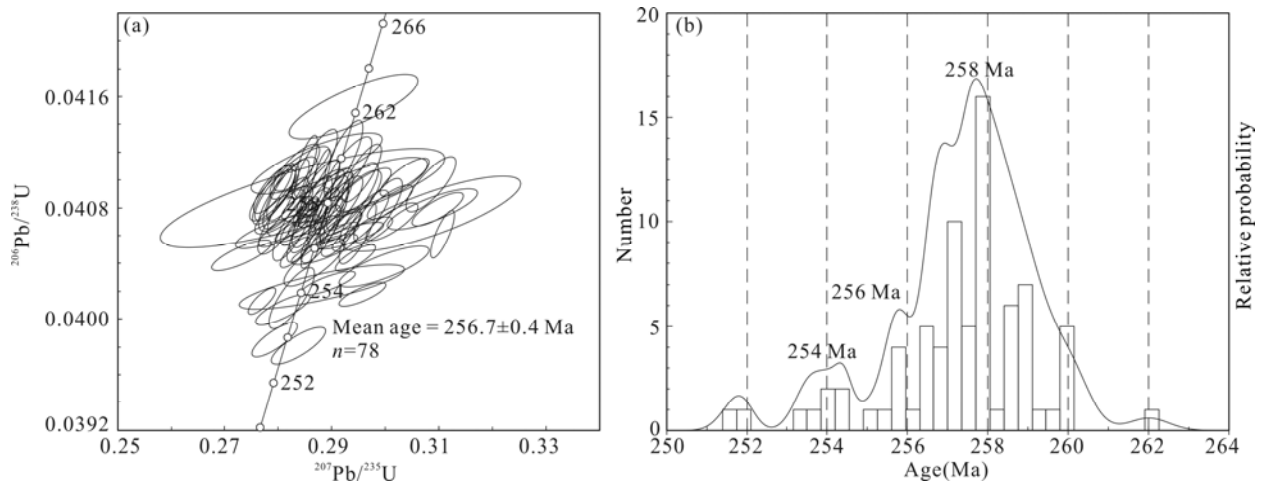


Fig. 8. Concordia plot (a), histogram and relative probability plot (b) for the sandstone (HLS2) from the Dajing section.

64 % of the total zircon grains analyzed date back to 256–258 Ma. The Th/U ratios and morphology of the zircons indicate that the source rocks were intermediate–acid magmatic rocks. Due to the fact that mafic rocks (basalt and diabase) contain rare zircons, the detrital zircons only record felsic magmatic rocks (Moecher and Samson, 2006; Malusà et al., 2016). Their subangular–angular shape shows that they were predominantly proximal. Therefore, the main sources of the Xuanwei Formation were Emeishan basalt, diabase, and intermediate–acid magmatic rocks (e.g., granite and syenite).

6.2 Implications for ELIP felsic volcanism

Most reported zircon U–Pb ages for magmatic rocks from the ELIP range from 266 Ma to 251 Ma (Shellnutt, 2014). 259 Ma U–Pb ages are dominant (e.g. Zhou et al., 2006; Zhong et al., 2007; Xu et al., 2008; Fan et al., 2008; Shellnutt et al., 2011), indicating that ELIP eruption peaked at this time.

Silicic volcanic rocks have only been reported from the top of the Emeishan volcanic succession and are restricted to Binchuan and Panzhuhua (Shellnutt and Jahn, 2010; Shellnutt and Zhou, 2008; Xu et al., 2010). Zircon U–Pb dating of these rocks has yielded weighted mean ages of 252 ± 2.5 Ma (Shellnutt and Zhou, 2008), 259.1 ± 0.5 Ma (Zhong et al., 2014), and ~ 260 Ma (Huang et al., 2016), which are later than the eruption of the Emeishan basalt.

Our studies suggest that long-term felsic magmatism may have occurred in the Upper Yangtze area. Our CL images of zircons suggest that they were derived from felsic magmatic rocks. The detrital zircon ages range from 262 Ma to 252 Ma, indicating that felsic volcanism occurred from 262 Ma and continued to 252 Ma. The histogram shows one peak value of 258 Ma, representing the main episode of silicic magmatism, after the basaltic ELIP volcanism.

6.3 Tectonic setting

LIPs are characteristic of volcanic rifted margins (Menzies et al., 2002). Volcanic rifted margins are easily distinguished from nonvolcanic margins, which do not contain a large amount of extrusive and/or intrusive igneous rock and may exhibit unusual features such as unroofed mantle peridotites (Pickup et al., 1996; Loudon and Chian, 1999).

Seismic investigations and the COMGRA-ELIP gravity experiment have shown that underplating and lithospheric thinning induced by a mantle plume occurred during the Emeishan basalt eruption (Chen et al., 2015, 2017; Deng et al., 2016; Xu et al., 2017). This supports the formation of the Emeishan basalt in a rift-related environment. The initiation of large igneous province is commonly a prerift phenomenon and takes the form of subaerial basaltic and/or silicic volcanism (Renne et al., 1992; Larsen and Saunders, 1998).

The prerift-to-synrift transition is marked by a structural change, in some cases a magmatic hiatus, erosion of newly formed rift mountains, and the formation of a high-velocity lower crust (HVLC) and a seaward-dipping reflector series (Mutter et al., 1982). The parallel unconformity between the Emeishan basalt and the Xuanwei Formation indicates this transition from prerift to synrift. The Xuanwei Formation conglomerates are also indicative of Emeishan basalt uplift.

The sedimentary environments of the Xuanwei Formation are successively alluvial fan, fluvial stream, and lacustrine (Shao et al., 2013), suggesting an extensional setting. This sedimentary development indicates that the period of plume-related uplift was very short and was associated with alluvial and fluvial deposition. Rifting was associated with uplift and fault tilting. During this phase, the sediments would have been sourced from the Emeishan basalt and felsic magmatic rocks, as supported by provenance analysis.

Furthermore, detrital zircon dating indicates that felsic magmatism occurred during the deposition of the Xuanwei Formation. Intrusions also occurred in the Upper Yangtze area, including pyroxene syenite (259.8±3.5 Ma; Xu et al., 2007), basic-ultrabasic rocks (259±3.0 Ma; Zhou et al., 2002), diorite (258±3.0 Ma; Zhou et al., 2006), granite (255±3.6 Ma; Xu et al., 2008), syenogranite (259.5±2.7 Ma; Zhong et al., 2011), diabase (255.4±3.1 Ma, 258.7±2.0 Ma; Zhong et al., 2011), syenite (259.2±0.4 Ma; Shellnutt et al., 2011), and syenite (252±2.5 Ma; Shellnutt and Zhou, 2008).

In addition, the available seismic tomography data show the presence of a thick (~20 km) HVLC ($V_p=7.1\text{--}7.8$ km/s) in the Yangtze Block (Liu et al., 2001), which may be genetically associated with the Emeishan LIP magmatism (Xu et al., 2004, 2007). HVLC is one of the principle diagnostic methods of a volcanic rifted margin (Menzies, et al., 2002).

Therefore, the tectonic setting of Xuanwei Formation deposition is interpreted to be a volcanic rifted margin. In the early stage of rifting, the crust became thinner because of domal uplift influenced by a mantle plume, and a graben was formed by subsidence. Alluvial fans consisting of conglomerates developed in the proximal area. On the basinward side, the sediments were mainly sandstones and mudstones that were deposited in fluvial rivers.

7 Conclusions

Here, the following conclusions are drawn on the basis of the sedimentary successions, heavy mineral analysis, and zircon U–Pb geochronology presented in this study: (1) The Xuanwei Formation was deposited by alluvial fans and fluvial rivers; (2) its provenance, as indicated by EPMA and zircon U–Pb dating, is Emeishan basalt and felsic magmatic rocks; and (3) it formed at a volcanic rifted margin, and felsic magmatism occurred continually in the Late Permian.

Acknowledgements

We thank Prof. Zhou Hongying from Tianjin

Geological Survey Centre for isotope dating. Special thanks to anonymous reviewers for their constructive comments and suggestions, which significantly improved the paper. This study was supported by the National Science Foundation of China (No. 41302080), the fundamental research funds for central public welfare research institutes (No: K1613) and Chinese Geological Survey (No. DD20190099, DD20190437).

Manuscript received Oct. 4, 2018

accepted Dec. 20, 2018

associate EIC XIAO Yitian

edited by LIU Lian

References

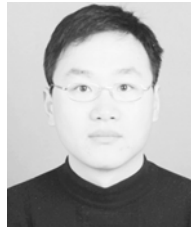
- Andersen, T., 2002. Correction of common lead in U–Pb analyses that do not report ^{204}Pb . *Chemical Geology*, 192(1–2): 59–79.
- Arai, S., 1992. Chemistry of chromian spinel in volcanic rocks as a potential guide to magma chemistry. *Mineralogical Magazine*, 56(383): 173–184.
- Barnes, S.J., and Roeder, P.L., 2001. The range of Spinel compositions in terrestrial mafic and ultramafic rocks. *Journal of Petrology*, 42(12): 2279–2302.
- Blair, T.C., 1999. Sedimentology of debris-flow-dominated warm spring Canyon alluvial fan, Death Valley, California. *Sedimentology*, 46(5): 941–965.
- Brandelik, A., 2009. CALCMIN – an EXCEL™ Visual Basic application for calculating mineral structural formulae from electron microprobe analyses. *Computers and Geosciences*, 35(7): 1540–1551.
- Chen, Y., Wang, Z.H., Guo, X., Deng, Y.F., Xu, T., Liao, X.F., Tian, X.B., Wu, J., Chen, L., Zhang, X., Tang, G.B., and Xu, Y.G., 2017. Geophysical signature of the ancient mantle plume activities: A case study of the Emeishan Large Igneous Province. *Bulletin of Mineralogy, Petrology and Geochemistry*, 36(3): 394–403 (in Chinese with English abstract).
- Chen, Y., Xu, Y.G., Xu, T., Si, S.K., Liang, X.F., Tian, X.B., Deng, Y.F., Chen, L., Wang, P., Xu, Y.H., Lan, H.Q., Xiao, F.H., Li, W., Zhang, X., Yuan, X.H., Badal, J., and Teng, J.W., 2015. Magmatic underplating and crustal growth in the Emeishan Large Igneous Province, SW China, revealed by a passive seismic experiment. *Earth and Planetary Science Letters*, 432: 103–114.
- Chung, S.L., and Jahn, B.M., 1995. Plume-lithosphere interaction in generation of the Emeishan flood basalts at the Permian-Triassic boundary. *Geology*, 23(10): 889–892.
- Coffin, M.F., and Eldholm, O., 1994. Large igneous provinces: Crustal structure, dimensions, and external consequences. *Review of Geophysics*, 32(1): 1–36.
- Collinson, J.D., 1996. Alluvial sediments. In: Reading, H.G. (eds.). *Sedimentary Environments and Facies*. Oxford: Blackwell Scientific Publications, 20–62.
- Cookinboo, H.O., Bustin, R.M., and Wilks, K.R., 1997. Detrital chromian spinel compositions used to reconstruct the tectonic setting of provenance; implications for orogeny in the Canadian Cordillera. *Journal of Sedimentary Research*, 67(1): 116–123.
- Corfu, F., Hanchar, J.M., Hoskin, P.W.O., and Kinny, P., 2003. Atlas of zircon textures. *Reviews in Mineralogy and Geochemistry*, 53(1): 469–500.
- Deng, Y.F., Chen, Y., Wang, P., Essa, K.S., Xu, T., Liang, X.F., and Badal, J., 2016. Magmatic underplating beneath the Emeishan large igneous province (South China) revealed by the COMGRA-ELIP experiment. *Tectonophysics*, 672–673: 16–23.
- Du, Q.X., Han, Z.C., Shen, X.L., Han, C., Song, Z.G., Gao, L.H., Han, M., Zhong, W.J., and Yan, J.L., 2017. New evidence of detrital zircon ages for the final closure time of the Paleo-Asian Ocean in the Eastern Central Asian Orogenic Belt (NE China). *Acta Geologica Sinica (English Edition)*, 91(5): 1910–

- 1914.
- Ernst, R.E., 2014. Large Igneous Provinces. Padstow: Cambridge University Press, 1–39.
- Fan, W.M., Wang, Y.J., Peng, T.P., Miao, L.C., and Guo, F., 2004. Ar–Ar and U–Pb geochronology of late Paleozoic basalts in western Guangxi and its constraints on the eruption age of Emeishan basalt magmatism. *Chinese Science Bulletin*, 49(21): 2318–2327.
- Fan, W.M., Zhang, C.H., Wang, Y.J., Guo, F., and Peng, T.P., 2008. Geochronology and geochemistry of Permian basalts in western Guangxi Province, Southwest China: Evidence for plume-lithosphere interaction. *Lithos*, 102(1–2): 218–236.
- Flood, Y.S., and Hampson, G.J., 2014. Facies and architectural analysis to interpret avulsion style and variability: Upper Cretaceous Blackhawk Formation, Wasatch Plateau, Central Utah, U.S.A. *Journal of Sedimentary Research*, 84(9): 743–762.
- Foix, N., Paredes, J.M., and Giacosa, R.E., 2013. Fluvial architecture variations linked to changes in accommodation space: Rio Chico Formation (Late Paleocene), Golfo San Jorge basin, Argentina. *Sedimentary Geology*, 294: 342–355.
- Gehrels, G.E., Johnsson, M.J., and Howell, D.G., 1999. Detrital zircon geochronology of the Adams argillite and Nation River Formation, East-Central Alaska, U.S.A. *Journal of Sedimentary Research*, 69(1): 135–144.
- He, B., Xu, Y.G., Huang, X.L., Luo, Z.Y., Shi, Y.R., Yang, Q.J., and Yu, S.Y., 2007. Age and duration of the Emeishan flood volcanism, SW China: Geochemistry and SHRIMP zircon U–Pb dating of silicic ignimbrites, post-volcanic Xuanwei Formation and clay tuff at the Chaotian section. *Earth and Planetary Science Letters*, 255(3–4): 306–323.
- He, B., Xu, Y.G., Xiao, L., and Wang, Y.M., 2003. Does the Panzhihua-Xichang rift exist?. *Geological Review*, 49(6): 572–52 (in Chinese with English abstract).
- He, B., Xu, Y.G., Xiao, L., Wang, Y.M., Wang, K.M., and Sha, S.L., 2006. Sedimentary responses to uplift of Emeishan mantle plume and its implications. *Geological Review*, 52(1): 32–37 (in Chinese with English abstract).
- He, B., Xu, Y.G., Zhong, Y.T., and Guan, J.P., 2010. The Guadalupian-Lopingian boundary mudstones at Chaotian (SW China) are clastic rocks rather than acidic tuffs: Implication for a temporal coincidence between the end-Guadalupian mass extinction and the Emeishan volcanism. *Lithos*, 119(1–2): 10–19.
- He, B.H., Liu, S.F., and Wu, P., 2017. LA–ICP–MS U–Pb geochronology and its geological implications of the detrital zircons from the lower strata of Upper Permian Xuanwei formation in Zhehai town, eastern Yunnan Province. *Geological Survey and Research*, 40(3): 126–133 (in Chinese with English abstract).
- Horn, B.L.D., Goldberg, K., and Schultz, C.L., 2018. Interpretation of massive sandstones in ephemeral fluvial settings: A case study from the Upper Candelária Sequence (Upper Triassic, Paraná Basin, Brazil). *Journal of South American Earth Sciences*, 81: 108–121.
- Huang, H., Cawood, P.A., Hou, M.C., Yang, J.H., Ni, S.J., Du, Y.S., Yan, Z.K., and Wang, J., 2016. Silicic ash beds bracket Emeishan Large Igneous province to <1 m.y. at ~ 260 Ma. *Lithos*, 264: 17–27.
- Jian, P., Liu, D.Y., Kröner, A., Zhang, Q., Wang, Y.Z., Sun, X.M., and Zhang, W., 2009. Devonian to Permian plate tectonic cycle of the Paleo-Tethys Orogen in southwest China (II): Insights from zircon ages of ophiolites, arc/back-arc assemblages and within-plate igneous rocks and generation of the Emeishan CFB province. *Lithos*, 113(3–4): 767–784.
- Kalsbeek, F., Frei, D., and Affaton, P., 2008. Constraints on provenance, stratigraphic correlation and structural context of the Volta basin, Ghana, from detrital zircon geochronology: An Amazonian connection? *Sedimentary Geology*, 212(1–4): 86–95.
- Kamenetsky, V.S., Crawford, A. J., and Meffer, S., 2001. Factors controlling chemistry of magmatic spinel: an empirical study of associated olivine, Cr-spinel and melt inclusions from primitive rocks. *Journal of Petrology*, 42(4): 655–671.
- Kang, Y., Chen, G., Xiao, X.Y., Ren, S.F., Zhang, W.G., and Shi, P.P., 2018. Detrital zircon U–Pb geochronology and its geological implication of the Nancaode and Zhuanghegou Formations in the southern margin Ordos Basin. *Acta Geologica Sinica*, 92(9): 1829–1842 (in Chinese with English abstract).
- Larsen, H.C., and Saunders, A., 1998. Scientific Results, Ocean Drilling Program, Leg 152: Tectonism and Volcanism at the Southeast Greenland Rifted Margin: A Record of Plume Impact and Later Continental Rupture. Texas: Ocean Drilling Program, 503–533.
- Lee, Y., 1999. Geotectonic significance of detrital chromian spinel: a review. *Geosciences Journal*, 3(1): 23–29.
- Lenaz, D., Kamenetsky, V.S., Crawford, A.J., and Princivalle, F., 2000. Melt inclusions in detrital spinel from the SE Alps (Italy–Slovenia): A new approach to provenance studies of sedimentary basins. *Contributions to Mineralogy and Petrology*, 139(6): 748–758.
- Lenaz, D., Mazzoli, C., Spišiak, J., Princivalle, F., and Maritan, L., 2009. Detrital Cr-spinel in the Šambron–Kamenica Zone (Slovakia): Evidence for an ocean-spreading zone in the Northern Vardar suture? *International Journal of Earth Sciences*, 98(2): 345–355.
- Lepvrier, C., Maluski, H., Tich, V.V., Leyreloup, A., Thi, P.T., and Vuong, N.V., 2004. The Early Triassic Indosinian orogeny in Vietnam (Truong Son Belt and Kontum Massif): implications for the geodynamic evolution of Indochina. *Tectonophysics*, 393(1–4): 87–118.
- Li, H.K., Geng, J.Z., Hao, S. Zhang, Y.Q., and Li, H.M., 2009. Zircon U–Pb dating technique using LA–MC–ICPMS. *Acta Mineralogica Sinica*, 29(supp.): 600–601 (in Chinese).
- Liu, C.Y. and Zhu, R.X., 2009. Geodynamic significances of the Emeishan basalts. *Earth Science Frontiers*, 16(2): 52–69.
- Liu, J.H., Liu, F.T., He, J.K., Chen, H., and You, Q.Y., 2001. Study of seismic tomography in Panxi paleorift area of southwestern China—structural features of crust and mantle and their evolution. *Science in China (D)*, 44(3), 277–288.
- Liu, Y.S., Gao, S., Hu, Z.C., Gao, C.G., Zong, K., and Wang, D.B., 2010. Continental and oceanic crust recycling-induced melt-peridotite interactions in the Trans-North China Orogen: U–Pb dating, Hf isotopes and trace elements in zircons from mantle xenoliths. *Journal of Petrology*, 51(1–2): 537–571.
- Louden, K.E., and Chian, D., 1999. The deep structure of non-volcanic rifted continental margin. *Philosophical Transactions of the Royal Society of London A: Mathematical, Physical and Engineering Sciences*, 357(1753): 767–804.
- Ludwig, K.R., 2003. User’s Manual for Isoplot 3.0: Geochronological Toolkit for Microsoft Excel. Berkeley: Berkeley Geochronology Center Special Publication, 4, 1–70.
- Luo, Z., Shao, L.Y., Yao, G.H. Deng, G.M., Wang, H., and Han, J., 2008. Mudstones in the Upper Permian coal-bearing series in eastern Yunnan and western Guizhou: Clay minerals composition and their environmental significance. *Journal of Palaeogeography*, 10(3): 297–304 (in Chinese with English abstract).
- Ma, Y.S., Chen, H.D., and Wang, G.L., 2009. Sequence Stratigraphy and Paleogeography in South China. Beijing: Science Press, 26–33 (in Chinese).
- Ma, Y.X., Zhang, C.J., Ji, X.T., and Ni, S.J., 2002. Tectono-magmatic model of Panxi paleo-rift. *Journal of Mineralogy and Petrology*, 22(1): 21–24 (in Chinese with English abstract).
- Mabi, A.W., Zhang, M.C., yang, Z.X., Li, Y.L., Wen, D.K., Liu, X.Y., 2017. Newly discovered fluvial-lacustrine sediments in the western Yangtze Block and their geological significance for the Emeishan Large Igneous Province. *Acta Geologica Sinica (English Edition)*, 91(2): 741–742.
- Malusà, M. G., Resentini, A., and Garzamti, E., 2016. Hydraulic sorting and mineral fertility bias in detrital geochronology. *Gondwana Research*, 31: 1–19.
- Martin, C.A.L., and Turner, B.R., 1998. Origin of massive-type sandstones in braided river systems. *Earth–Science Reviews*, 44(1): 15–38.
- Menzies, M.A., Klemperer, S.L., Ebinger, C.J., and Baker, J., 2002. Characteristics of volcanic rifted margins. In Menzies, M.A., Klemperer, S.L., Ebinger, C.J., Baker, J. (eds.).

- Volcanic Rifted Margin. New York: Geological Society of America Special Paper, 362, 1–15.
- Miall, A., 1996. The Geology of Fluvial Deposits—Sedimentary Facies, Basin Analysis and Petroleum Geology. Berlin: Springer-Verlag, 99–130.
- Moecher, D.P. and Samson, S.D., 2006. Differential zircon fertility of source terranes and natural bias in the detrital zircon record: Implications for sedimentary provenance analysis. *Earth and Planetary Science Letters*, 247(3–4): 252–266.
- Mutter, J., Talwani, M., and Stoffa, P.L., 1982. Origin of seaward-dipping reflectors in oceanic crust off the Norwegian margin by “subaerial sea-floor spreading”. *Geology*, 10(7): 353–357.
- Nadon, G.C., 1994. The genesis and recognition of anastomosed fluvial deposits: data from the St. Mary River Formation, Southwestern Alberta, Canada. *Journal of Sedimentary Research*, B64(4): 451–463.
- Naipauer, M., Vujovich, G.I., Cingolani, C.A., and McClelland, W.C., 2010. Detrital zircon analysis from the Neoproterozoic-Cambrian sedimentary cover (Cuyania terrane), Sierra de Pie de Palo, Argentina: Evidence of a rift and passive margin system? *Journal of South American Earth Sciences*, 29(2): 306–326.
- Nelson, J., and Gehrels, G., 2007. Detrital zircon geochronology and provenance of the southeastern Yukon-Tanana terran. *Canadian Journal of Earth Sciences*, 44(3): 297–316.
- Nemec, W., and Postma, G., 1993. Quaternary alluvial fans in southern Grete: sedimentation process and geomorphic evolution. In Marzo, M., and Puigdefabregas, C. (eds.). *Alluvial Sedimentation*. Oxford: Blackwell Science, 235–276.
- Nemec, W., and Steel, R.J., 1984. Alluvial and coastal conglomerates: their significance features and some comments on gravelly mass-flow deposits. In: Koster, E.H., and Steel, R.J. (eds.). *Sedimentology of Gravels and Conglomerates*. Calgary: Canadian Society of Petroleum Geologists Memoir, 10, 1–31.
- Pickup, S.L.B., Whitmarsh, R.B., Fowler, C.M.R., and Reston, T.J., 1996. Insight into the nature of the ocean-continent transition off West Iberia from a deep multichannel seismic reflection profile. *Geology*, 24(12): 1079–1082.
- Renne, P., Ernesto, M., Pacca, I.G., Coe, R.S., Glen, J.M., Prevot, M., and Perrin, M., 1992. The age of Paraná flood volcanism, rifting of Gondwanaland and the Jurassic-Cretaceous boundary. *Science*, 258(5084): 975–979.
- Rubatto, D., and Gebauer D., 2000. Use of cathodoluminescence for U–Pb zircon dating by ion microprobe: some examples from the Western Alps. In: Pagel, M., Barbin, V., and Blanc, P. (eds.). *Cathodoluminescence in Geosciences*. Berlin Heidelberg New York: Springer, 373–400.
- Rust, B.R., 1978. Depositional models for braided stream. In: Miall, A.D. (ed.). *Fluvial Sedimentology*. Calgary: Canadian Society of Petroleum Geologists Memoir, 5, 605–625.
- Shao, L.Y., Gao, C.X., Zhang, C., Wang, H., Guo, L.J., and Gao, C.H., 2013. Sequence-palaeogeography and coal accumulation of late Permian in Southwestern China. *Acta Sedimentologica Sinica*, 31(5): 856–866 (in Chinese with English abstract).
- Shao, L.Y., Liu, H.M., Tian, B.L., and Zhang, P.F., 1998. Sedimentary evolution and its controls on coal accumulation for the late Permian in the Upper Yangtze area. *Acta Sedimentologica Sinica*, 16(2): 55–60 (in Chinese with English abstract).
- Shao, L.Y., Zhang, C., Yan, Z.M., Dong, D.X., Gao, C.X., Li, Y.J., Xu, X.Y., Liang, W.L., Yi, T.S., Xu, X.H., Li, G.M., Chen, Z.S., and Cheng, A.G., 2016. Sequence-palaeogeography and coal accumulation of the Late Permian in South China. *Journal of Palaeogeography*, 18(6): 905–919 (in Chinese with English abstract).
- Shao, L.Y., Zhang, P.F., Chen, D.Z., and Luo, Z., 1994. Braided delta depositional system and coal accumulation during early Late Permian period in eastern Yunnan and western Guizhou, Southwest China. *Acta Sedimentologica Sinica*, 12(4): 132–139 (in Chinese with English abstract).
- Shellnutt, J.G., and Jahn, B.M., 2010. Formation of the Late Permian Panzhihua plutonic-hypabyssal-volcanic igneous complex: Implications for the genesis of Fe-Ti oxide deposits and A-type granites of SW China. *Earth and Planetary Science Letters*, 289(3–4), 509–519.
- Shellnutt, J.G., and Zhou, M.F., 2008. Permian, rifting related fayalite syenite in the Panxi region, SW China. *Lithos*, 101(1–2): 54–73.
- Shellnutt, J.G., 2014. The Emeishan large igneous province: A synthesis. *Geoscience Frontiers*, 5(3): 369–394.
- Shellnutt, J.G., Usuke, T., Kennedy, A.K., and Chiu, H.Y., 2015. A lower crust origin of some flood basalts of the Emeishan large igneous province, SW China. *Journal of Asian Earth Sciences*, 109: 74–85.
- Shellnutt, J.G., Wang, K.L., Zellmer, G.F., Iizuka, Y., Jahn, B.M., Pang, K.N., Qi, L., and Zhou, M.F., 2011. Three Fe-Ti oxide ore-bearing gabbro-granitoid complexes in the Panxi region of the Permian Emeishan large igneous province, SW China. *American Journal of Science*, 311(9): 773–812.
- Shultz, A.W., 1984. Subaerial debris-flow deposition in the Upper Paleozoic Cutler Formation, Western Colorado. *Journal of Sedimentary Research*, 54(3): 749–772.
- Sircombe, K.N., 1999. Tracing provenance through the isotope ages of littoral and sedimentary detrital zircon, eastern Australia. *Sedimentary Geology*, 124(1–4): 47–67.
- Song, X.Y., Zhou, M.F., Cao, Z.M., and Robinson, P.T., 2004. Late Permian rifting of the South China Craton caused by the Emeishan mantle plume? *Journal of the Geological Society*, 161(5): 773–781.
- Tan, T.K., 1987. Geodynamics and tectonic evolution of the Panxi rift. *Tectonophysics*, 133(3–4): 287–304.
- Udden, J.A., 1914. Mechanical composition of clastic sediments. *Geological Society of America Bulletin*, 25(1): 655–744.
- Wang, Y.S., and Li, Y.G., 1996. Formation and evolution of the Xichang Basin. *Journal of Chengdu University of Technology*, 23(1): 85–90 (in Chinese with English abstract).
- Wentworth, C.K., 1922. A scale of grade and class terms for clastic sediments. *The Journal of Geology*, 30(5): 377–392.
- Wu, G.Y., 1997. Tectonic evolution of Panzhihua-Xichang paleorift during Late Palaeozoic. *Journal of Chengdu University of Technology*, 24(2): 52–57 (in Chinese with English abstract).
- Xu, X.S., Liu, B.J., and Zhao, Y.G., 1996. Sequence boundary genesis and basin-mountain transformation on the western margin of the Upper Yangtze Platform during the Permian to Triassic. *Tethyan Geology*, 16(20): 1–30 (in Chinese with English abstract).
- Xu, Y.G., Chung, S.L., Jahn, B.M., and Wu, G.Y., 2001. Petrologic and geochemical constraints on the petrogenesis of Permian-Triassic Emeishan flood basalts in southwestern China. *Lithos*, 58(3–4): 145–168.
- Xu, Y.G., Chung, S.L., Shao, H., and He, B., 2010. Silicic magmas from the Emeishan large igneous province, Southwest China: Petrogenesis and their link with the end-Guadalupian biological crisis. *Lithos*, 119(1–2): 47–60.
- Xu, Y.G., He, B., Chung, S.L., Menzies, M.A., and Frey, F.A., 2004. Geologic, geochemical, and geophysical consequences of plume involvement in the Emeishan flood-basalt province. *Geology*, 32(10): 917–920.
- Xu, Y.G., He, B., Huang, X.L., Luo, Z.Y., Chung, S.L., Xiao, L., Zhu, D., Shao, H., Fan, W.M., Xu, J.F., and Wang, Y.J., 2007. Identification of mantle plumes in the Emeishan Large Igneous Province. *Episodes*, 30(1): 32–42.
- Xu, Y.G., He, B., Luo, Z.Y., and Liu, H.Q., 2013. Study of mantle plume and large igneous provinces in China: An overview and perspectives. *Bulletin of Mineralogy, Petrology and Geochemistry*, 32(1): 25–39 (in Chinese with English abstract).
- Xu, Y.G., Luo, Z.Y., Huang, X.L., He, B., Xiao, L., Xie, L.W., and Shi, Y.R., 2008. Zircon U-Pb and Hf isotope constraints on crustal melting associated with the Emeishan mantle plume. *Geochimica et Cosmochimica Acta*, 72(13): 3084–3104.
- Xu, Y.G., Zhong, Y.T., Wei, X., Chen, J., Liu, H.Q., Xie, W., Luo, Z.Y., Li, H.Y., He, B., Huang, X.L., Wang, Y., and Chen, Y., 2017. Permian mantle plumes and Earth’s surface

- system evolution. *Bulletin of Mineralogy, Petrology and Geochemistry*, 36(3): 359–373 (in Chinese with English abstract).
- Yan, Y.J., and Wu, Y.L., 1996. Evolution of the Bayan Har-West Sichuan peripheral foreland basin in southwestern China. *Sedimentary Facies and Palaeogeography*, 16(3): 16–29 (in Chinese with English abstract).
- Yang, J.H., Cawood, P.A., and Du, Y.S., 2015. Voluminous silicic eruptions during late Permian Emeishan igneous province and link to climate cooling. *Earth and Planetary Science Letters*, 432: 166–175.
- Zhang, Z.C., and Wang, F.S., 2004. High-Mg olivines and high-Cr spinels in the picritic from the Emeishan continental flood basalt province. *Progress in Natural Science*, 14(1): 70–74 (in Chinese with English abstract).
- Zhang, Z.W., Yang, X.Y., Li, S., and Zhang, Z.S., 2010. Geochemical characteristics of the Xuanwei Formation in West Guizhou: Significance of sedimentary environment and mineralization. *Chinese Journal of Geochemistry*, 29(4): 355–364.
- Zhao, L.X., Dai, S.F., Graham, I.T., Li, X., and Zhang, B.B., 2016. New insights into the lowest Xuanwei Formation in eastern Yunnan Province, SW China: Implications for Emeishan large igneous province felsic tuff deposition and the cause of the end-Guadalupian mass extinction. *Lithos*, 264: 375–391.
- Zheng, X., and Wang, W.H., 2015. Analysis of coal accumulating environment of Xuanwei Formation in South Sichuan area. *Coal Technology*, 34(4): 113–114 (in Chinese with English abstract).
- Zhong, H., Campbell, I.H., Zhu, W.G., Allen, C.M., Hu, R.Z., Xie, L.W., and He, D.F., 2011. Timing and source constraints on the relationship between mafic and felsic intrusions in the Emeishan large igneous province. *Geochimica et Cosmochimica Acta*, 75(5): 1374–1395.
- Zhong, H., Zhu, W.G., Chu, Z.Y., He, D.F., and Song, X.Y., 2007. Shrimp U–Pb zircon geochronology, geochemistry, and Nd–Sr isotopic study of contrasting granites in the Emeishan large igneous province, SW China. *Chemical Geology*, 236(1–2): 112–133.
- Zhong, Y.T., He, B., Mundil, R., and Xu, Y.G., 2014. CA–TIMS zircon U–Pb dating of felsic ignimbrite from the Binchuan section: Implications for the termination age of Emeishan large igneous province. *Lithos*, 204: 14–19.
- Zhou, M.F., Malpas, J., Song, X.Y., Robinson, P.T., Sun, M., Kennedy, A.K., Leshner, M.C., and Keays, R.R., 2002. A temporal link between the Emeishan large igneous province (SW China) and the end-Guadalupian mass extinction. *Earth and Planetary Science Letters*, 196(3–4): 113–122.
- Zhou, M.F., Zhao, J.H., Qi, L., Su, W.C., and Hu, R.Z., 2006. Zircon U–Pb geochronology and elemental and Sr–Nd isotope geochemistry of Permian mafic rocks in the Funing area, SW China. *Contributions to Mineralogy and Petrology*, 151(1): 1–19.
- Zhou, M.K., and Liu, Y.R., 1988. *The Geological Tectonic Characteristics and Evolution in Xichang-Mid-Yunnan Region*. Chongqing: Chongqing Publishing House, 1–199 (in Chinese).

About the first and corresponding author



ZHANG Yingli, Male; born in 1979; doctor; graduated from Institute of Geology and Geophysics, Chinese Academy of Sciences; associate professor of Institute of Mineral Resources, Chinese Academy of Geological Sciences. He is now interested in the study on basin tectonic and sedimentology. E-Mail: yinglizh@126.com. Phone: 010-68999915, 13371602654.